

Revealing Actual Viscoelastic Relaxation Times in Capillary Breakup

Nan Hu,^{1,*} Jonghyun Hwang,¹ Tachin Ruangkriengsin,² and Howard A. Stone^{1,†}

¹*Department of Mechanical and Aerospace Engineering, Princeton University, NJ 08544, USA*

²*Program in Applied and Computational Mathematics, Princeton University, NJ 08544, USA*

(Dated: March 11, 2025)

We use experiments and theory to elucidate the size effect in capillary breakup rheometry, where pre-stretching in the visco-capillary stage causes the apparent relaxation time to be consistently smaller than the actual value. We propose a method accounting for both the experimental size and the finite extensibility of polymers to extract the actual relaxation time. A phase diagram characterizes the expected measurement variability and delineates scaling law conditions. The results refine capillary breakup rheometry for viscoelastic fluids and advance the understanding of breakup dynamics across scales.

Capillary thinning and breakup of viscoelastic liquid threads are ubiquitous in natural environments, biological tissues, and industrial applications [1–3]. Unlike viscous liquids, the capillary breakup of viscoelastic liquids exhibits distinct behaviors such as the exponential decay of filament thinning [4–7] and the formation of satellite droplets on a string [8–11], which are attributed to the elastic forces from polymeric stresses. Consequently, capillary breakup rheometry, which leverages these dynamic characteristics, has been a method widely used to measure viscoelastic properties, and is especially promising for weakly-elastic fluids [12] and biopolymers such as DNA [13, 14], whose properties are difficult to measure using common rheometric methods. Current well-developed experimental techniques include stretching a liquid bridge between two plates (known as CaBER) [15–18], jetting [19–22], dripping [23, 24], and dripping-onto-substrate (DoS) [25–28].

Typically, the capillary breakup of viscoelastic fluids is governed by the interplay of inertial, viscous, elastic, and surface tension forces. Based on the sequence of events during the breakup of droplets or liquid bridges, the dynamics can be categorized into the visco-capillary (VC) or inertial-capillary (IC) stage, the elasto-capillary (EC) stage, and the final visco-elasto-capillary (VEC) stage [29]. By assuming infinite extensibility of the polymer chains ($b = \infty$) with a (longest) relaxation time λ , the evolution of the neck diameter $D(t)$ for the EC stage is well-known as

$$D(t)/D_1 = (GD_1/2\gamma)^{1/3} \exp[-(t - t_1)/3\lambda], \quad (1)$$

where G is the modulus of the viscoelastic fluid, D_1 is the initial diameter of the liquid filament, γ is the surface tension, and t_1 is the time of onset of the EC stage [4]. This formula has been adopted in numerous studies to interpret the experimental results of the variation of the filament diameter $D(t)$ during the EC stage. Thus, one obtains an estimate of the apparent relaxation time λ_e for various kinds of polymer solutions by fitting the exponential decay [12, 15, 25–27, 29–32].

However, recent studies have found that pre-stretching of the polymers or filament thinning during the IC/VC

stage significantly influences the exponential decay in the subsequent EC stage [14, 17, 18, 23, 32]. Such initial conditions for elasto-capillary thinning can be influenced by multiple parameters, including the initial separation rate of the plates [17] and the initial diameter D_0 of the liquid bridge [18] in the CaBER method, various nozzle diameters ℓ in the dripping method (e.g., experiments indicate $\lambda_e \propto \ell^{8/9}$) [23], and different values of the extensibility parameter, b , of the polymer in the DoS method [32]. This dependence introduces a strong sensitivity of the extracted relaxation time λ_e on the initial conditions and inevitable pre-stretching effects that occur in capillary breakup rheometry. To date, there are only a few studies that have indicated the effect of pre-stretching on the apparent relaxation time λ_e [18, 23, 32], though no studies have identified the actual relaxation time λ from capillary breakup measurements, as well as a scaling law of λ_e versus ℓ or D_0 .

In this Letter we demonstrate that size-dependent apparent relaxation times, λ_e , obtained from capillary breakup processes of varying scales, can be used to estimate the actual relaxation time, λ , while simultaneously determining the extensibility, b , representative of the polymer solution. In particular, accounting for finite extensibility b , we show that pre-stretching during the VC stage shortens the exponential decay in the elasto-capillary stage, leading to $\lambda_e < \lambda$, and that this effect can be dependent on the size of the experimental setups. Through experiments and numerical solutions, we unravel this quantitative relationship, enabling the determination of the actual relaxation time λ from both our measurements and those reported in recent studies.

The capillary breakup processes considered here include dripping, DoS, and CaBER (Fig. 1a (i, ii, iii)). In all cases, the liquid initially is slowly stretched in a quasi-static manner within devices of characteristic size ℓ . Under the action of capillary forces driving the Rayleigh-Plateau instability, the liquid rapidly contracts from the initial diameter D_0 of the VC stage to the initial diameter D_1 of the EC stage. In our experiments, we used needles with varying outer diameter $\ell \in \{0.3, 0.5, 0.9, 1.8, 2.4\}$ mm (corresponding to 30G, 25G, 20G, 15G, and 13G

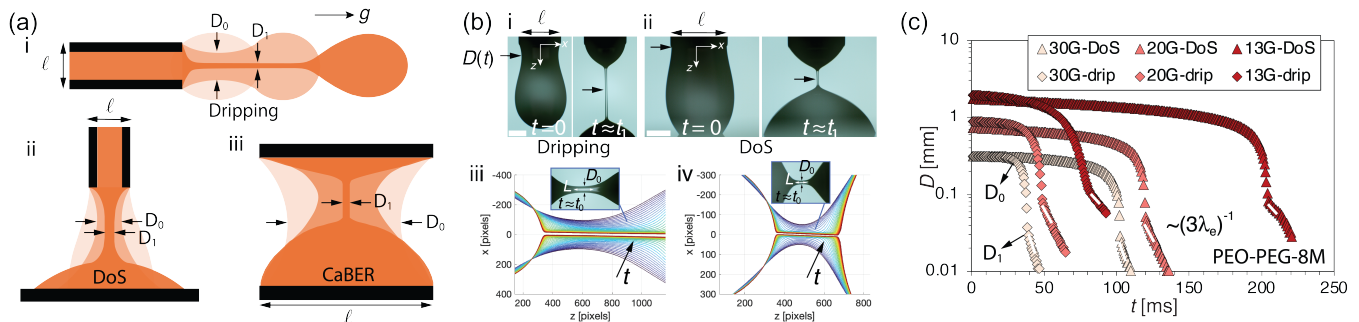


FIG. 1. Capillary breakup rheometry. (a) Schematic illustrations of liquid filament breakup for different experimental configurations: (i) dripping, (ii) dripping-onto-substrate (DoS), and (iii) a liquid bridge between two plates (classic CaBER). The liquid is initially held quasi-steady by a nozzle or plates with diameter ℓ . The minimum neck diameter of the liquid, $D(t)$, evolves over time from the D_0 to D_1 , where subscripts 0 and 1 mark the onset of the VC and EC stages, respectively. (b) Representative measurements for a PEO-PEG-8M solution using (i) dripping and (ii) DoS methods with a 13G nozzle ($\ell = 2.4$ mm). (iii) and (iv) are the extracted evolutions of interface shapes with increasing time t corresponding, respectively, to dripping and DoS, where D_0 is estimated by taking the filament aspect ratio $1 \lesssim L/D_0 \lesssim 3$. Scale bars represent 1 mm. (c) Representative datasets showing the variation of $D(t)$ for different $\ell \in \{0.3, 0.9, 2.4\}$ mm and methods (different symbols). Distinct slopes of $\log_{10} D$ in the EC stage for varying ℓ indicate a size-dependent apparent relaxation time λ_e predicted by the slope $\sim (3\lambda_e)^{-1}$.

needles) to conduct tests using the dripping and DoS methods. Given that the influence of size of the CaBER method has been tested in Ref. [18], we also used their data of the PEOvis solution (see [33], §I and Fig. S1) for our analysis.

Three kinds of polymer solutions were employed in our experiments: PIB-PB (polyisobutylene dissolved in a polybutene-mineral oil mixed solvent), PS-DOP (polystyrene dissolved in the organic solvent dioctyl phthalate), and PEO-PEG (polyethylene oxide dissolved in a polyethylene glycol-water solution), whereas PIB-PB-0.3 and PIB-PB-0.02 denote different PIB concentrations; PEO-PEG-8M and PEO-PEG-1M identify different molecular weights of PEO. These latter fluids can be regarded as Boger fluids with constant viscosity (Fig. S2 [33]), ensuring that additional effects from viscosity variations with extension rate are eliminated. Detailed preparation procedures and physical property measurements, such as viscosity η_0 , surface tension γ , storage modulus G' , and loss modulus G'' , are provided in [33] §II and summarized in Table S1.

Capillary breakup tests were conducted inside a transparent chamber to shield the system from air disturbances, with a liquid reservoir included to minimize the effects of evaporation (see [33] §III). High-speed imaging was conducted using a camera (VEO 640L, Phantom) equipped with microscope objectives (Nikon) of 2X, 5X, or 10X magnifications to accommodate varying nozzle diameters. A syringe pump (PHD 2000, Harvard Apparatus) controlled the flow rate at $Q = 1 - 10 \mu\text{L}/\text{min}$, ensuring a quasi-static droplet for dripping. Taking the PEO-PEG-8M solution as an example, representative snapshots from the dripping and DoS tests, captured at a resolution of 2560×1600 pixels and 1500 frames per second (fps), are shown in Fig. 1(b-i, ii), respectively. The

liquid surface was analyzed using a custom MATLAB image-processing algorithm to track the gas-liquid interface as depicted in Fig. 1(b-iii, iv), in order to obtain the evolution of the minimum neck diameter $D(t)$ (Fig. 1c). Unlike the CaBER method, where the instability can be triggered in a controlled manner by adjusting the plate spacing to directly determine D_0 , we propose that in the dripping and DoS methods, D_0 should be determined by ensuring $1 \lesssim L/D_0 \lesssim 3$ (Fig. 1b-iii, iv, detailed discussion seen in [33] §V). Each case was repeated at least three times to confirm data reproducibility. The results for the other solutions are provided in Fig. S4 [33].

The transition in the $D(t)$ curves and the appearance of a uniform filament (Fig. 1b-i, ii) allow the determination of the initial diameter D_1 for the EC stage. Using Eq. (1), a fit following this point (white lines in Fig. 1c) yields the value of λ_e . The results show that λ_e increases with the nozzle diameter ℓ , though no significant difference is observed between the λ_e values obtained from the dripping and DoS methods. We conducted a comprehensive comparison of the apparent relaxation times λ_e for different viscoelastic fluids, nozzle diameters ℓ , and testing methods (Fig. 2). We observed that PEO-PEG, PIB-PB-0.02, and PEOvis solutions exhibit a size dependence of λ_e , showing a variation from $\sim \ell$ to $\sim \ell^{0.5}$ with increasing ℓ for one fluid. In contrast, λ_e values of the PS-DOP and PIB-PB-0.3 solution remain nearly constant.

We believe that viscoelastic fluids formed from nearly monodisperse polymer solutions should exhibit a constant intrinsic (longest) relaxation time λ , independent of testing conditions; indeed, this is the most common description of these solutions. To uncover the underlying dependence of λ_e on experimental size ℓ , we employed a zero-dimensional model based on the FENE-P model to predict the evolution of the dimensionless filament diam-

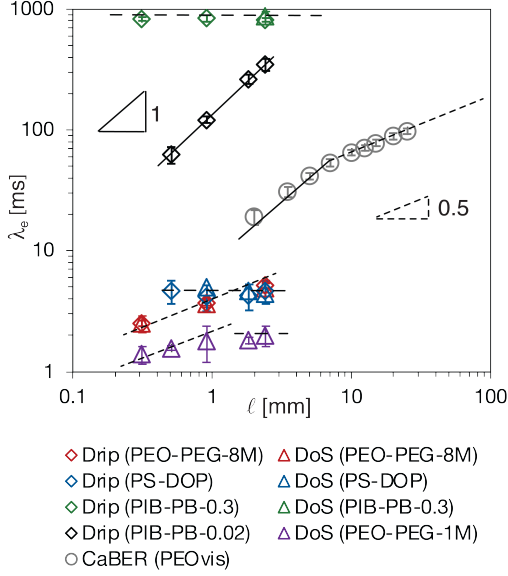


FIG. 2. Dependence of apparent relaxation time λ_e on apparatus size ℓ for different Boger fluids using specific methods: PEO-PEG, PS-DOP, PIB-PB in this work by dripping and/or DoS, and PEOvis (Ref. [18]) by CaBER.

eter $a(\tau) = D(\tau)/D_0$, according to equations for mass and momentum balances (subscripts s and p denote, respectively, solvent and polymer), and microstructure evolution along the axial (z) and radial (r) directions,

$$\frac{1}{Ec} \frac{1}{a} = \frac{3\beta}{1-\beta} E + f(A_{zz} - A_{rr}) \quad (2a)$$

$$\partial_\tau A_{zz} = (2E - f) A_{zz} + 1 \quad (2b)$$

$$\partial_\tau A_{rr} = (-E - f) A_{rr} + 1 \quad (2c)$$

$$\partial_\tau a = -\frac{aE}{2}, \quad (2d)$$

where we have introduced dimensionless time $\tau = t/\lambda$, elasto-capillary number $Ec = \eta_p D_0 / 2\lambda\gamma$, solvent viscosity ratio $\beta = \eta_s / \eta_0$, dimensionless (time-varying) extensional strain rate $E = -2\lambda D^{-1} \frac{dD}{dt}$, the conformation tensor \mathbf{A} with rr and zz components, and the finite extensibility function $f = (b-3)/(b-A_{zz}-2A_{rr})$. By comparing simplified analytical solutions (see [33] §IV-B1, B2), approximate solutions ([33] §IV-B3), and an analysis of the full model ([33] §IV-C1) under different assumptions, we demonstrated that the evolution is sensitive to the initial conformation $\mathbf{A}(t_1)$ for the EC stage. Only by solving the full model numerically can the variations in the VC, EC, and VC-EC transitions be captured accurately (see [33] §IV).

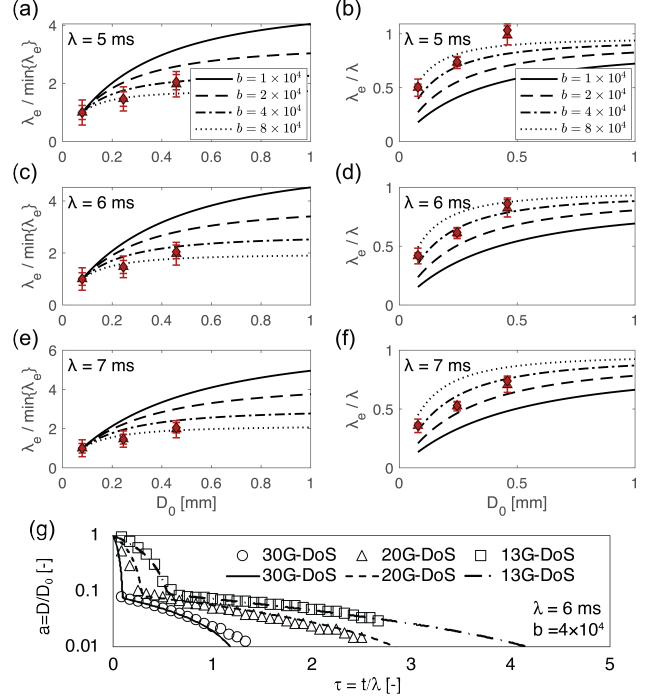


FIG. 3. Prediction of the relaxation time ratio $\lambda_e / \min\{\lambda_e\}$ (a, c, e) and relative ratio λ_e / λ (b, d, f) versus the initial diameter D_0 for the PEO-PEG-8M solution, assuming $\lambda = 5$ ms (a, b), 6 ms (c, d), and 9 ms (e, f), with varying extensibility $b \in \{2 \times 10^4, 4 \times 10^4, 8 \times 10^4\}$. The symbols represent experimental results of λ_e obtained from the dripping and DoS methods, suggesting a good approximation of $\lambda \approx 6$ ms and simultaneously indicating $b \approx 4 \times 10^4$ for the PEO-PEG solution. (g) Comparison of experimental and numerical results using $(\lambda, b) = (6 \text{ ms}, 4 \times 10^4)$ for three different diameter needles.

With the initial conditions $a = A_{rr} = A_{zz} = 1$, Eqs. (2) can be solved numerically ([33] §IV-C2) using MATLAB's ODE15s solver to yield the temporal evolution of the dimensionless diameter $a(\tau)$, conformation A_{zz} and A_{rr} , and extensional strain rate $E(\tau)$ (typical results are shown in Fig. 3 for $a(\tau)$; see also Fig. S10 for all variables). Based on the numerical results, we calculate the numerically predicted $\lambda_e / \lambda = \max\{2/(3E(t))\}$ for $t \geq t_1$, which corresponds to the early period of the EC stage (see [33], Fig. S10d), under various parameter choices of β , Ec , and b . This further allows the construction of a phase diagram of λ_e / λ as a function of the three parameters (see [33], Fig. S10e). Notably, every fixed β enables the phase diagram to be approximated with a two-dimensional representation in terms of Ec and b (see [33], Fig. S10f).

For a specific viscoelastic liquid, as properties η_p , β and γ are measurable and size D_0 is controlled, we can assume a true relaxation time λ for determining Ec in Eq. (2a), and explore a wide range of b values in the numerical calculations. Taking the PEO-PEG solution as an example,

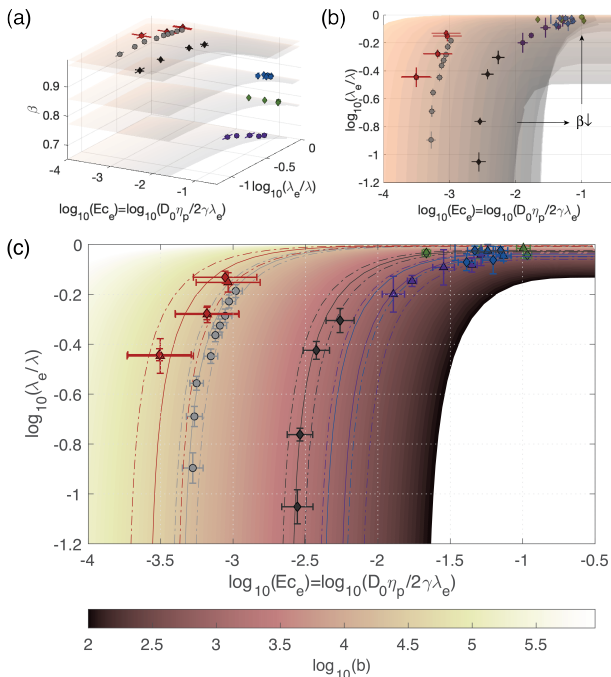


FIG. 4. Dimensionless map of the relaxation time ratio λ_e/λ versus the measurable elasto-capillary number $Ec_e = D_0 \eta_p / (2\gamma \lambda_e)$ for various unknown extensibility values $b \in [10^2, 10^6]$. (a) 3D maps for different β of a specific solution. (b) Top view of 3D maps. (c) Collapsed 2D map for easy comparison. The symbols represent experimental results (red: PEO-PEG-8M, purple: PEO-PEG-1M, green: PIB-PB-0.3, black: PIB-PB-0.02, blue: PS-DOP) and Ref. [18] (gray: PEOvis). Solid lines are obtained from fitting, with deviation ranges enclosed by dash-dot lines, suggesting the estimations.

numerical predictions of the relative ratio $\lambda_e/\min\{\lambda_e\}$ (Fig. 3a, c, e) and λ_e/λ (Fig. 3b, d, f) for assumed $\lambda \in \{5, 6, 7\}$ ms and $b \in \{10^4, 2 \times 10^4, 4 \times 10^4, 8 \times 10^4\}$ are compared with experimental results (symbols in Fig. 3). The trend of $\lambda_e/\min\{\lambda_e\}$ for different D_0 values provides a significant indicator for comparison with model predictions because both λ_e/λ and $\lambda_e/\min\{\lambda_e\}$ are uniquely determined for fixed Ec_e and β .

The comparisons of the two trends indicate that when $\lambda \approx 6$ ms, the numerical predictions align well with the experimental results (dash-dot curves in Fig. 3g). Furthermore, at the same time this analysis determines $b \approx 4 \times 10^4$. We emphasize that with this approach, only λ needs to be adjusted for comparison, while b is determined through the matching of the two trends. The comparison of experimental and numerical $a(\tau)$ shown in Fig. 3g suggests a good estimation for λ and b has been achieved. The same procedure was used to find a good agreement with the experimental data from [18] (Fig. S11 in [33]).

Next, we analyzed the experimental data presented in Fig. 2 and constructed a dimensionless phase diagram

(note the logarithmic axes) of λ_e/λ as a function of Ec_e , b and β (Fig. 4a), where $Ec_e = D_0 \eta_p / (2\gamma \lambda_e)$, with each variable being directly measurable from experiments. Although different β values affect the map, particularly for small b , indicated in Fig. 4b, we can construct the phase diagram with all experimental data as shown in Fig. 4c; uncertainties in all measurable parameters were considered to determine the true relaxation time λ and the range of extensibility b for each viscoelastic fluid tested.

For the PEO-PEG-8M solution, the relaxation time is estimated as $\lambda \approx 6$ ms, with $b = 4 \times 10^4 \pm 0.2$. For the PEOvis solution, $\lambda \approx 150$ ms and $b = 2 \times 10^4 \pm 0.1$, consistent with the results from Ref. [18], where $b \approx 2 \times 10^4$ was estimated using an additional model. This agreement reinforces the validity of our approach. Furthermore, the larger b for PEO-PEG-8M compared to PEOvis aligns with their respective molecular weights, $M_w \sim 8 \times 10^6$ in our experiments versus $M_w \sim 4 \times 10^6$ in Ref. [18], given similar solvent mixtures (see [33], Tab. S1). This observation is further supported by the PEO-PEG-1M solution with $M_w \sim 1 \times 10^6$, which yields $(\lambda, b) \approx (2.2 \text{ ms}, 7 \times 10^2 \pm 0.2)$.

For the PIB-PB-0.3 solution, experimental uncertainties prevent a precise determination of whether λ_e varies with D_0 , suggesting that a reasonable estimation of λ and b is not readily attainable. However, utilizing the more dilute PIB-PB-0.02 solution, we estimate $(\lambda, b) \approx (700 \text{ ms}, 2 \times 10^3 \pm 0.1)$. Given that both solutions contain the same polymer at different dilutions, it is reasonable to assume that b remains unchanged. This leads to an inferred relaxation time of $\lambda \approx 850$ ms for PIB-PB-0.3.

From the phase diagram (Fig. 4), two distinct regions can be identified. When $\log_{10}(Ec_e b) \gtrsim 1.5$, the experimentally measured λ_e becomes independent of the experimental size, i.e. $\lambda_e \sim \ell^0$. However, this does not imply that the true relaxation time λ is obtained. In this region, since b cannot be experimentally fitted, an additional evaluation of b is necessary to determine the specific value of λ_e/λ . In the region where $\log_{10}(\lambda_e/\lambda) \lesssim -0.6$, the slope of $\log_{10}(\lambda_e/\lambda)$ approaches infinity, indicating that $\lambda_e \sim D_0$. This is consistent with the scaling law $\lambda_e \sim \ell$ observed in Fig. 2 when $\ell(D_0)$ becomes sufficiently small. The $\lambda_e \sim \ell^{0.5}$ scaling law observed in Fig. 2 represents an empirical scaling behavior characterizing the transition between the two regions.

Thus, some predictions can be made. For fluids with relatively low surface tension and strong viscoelasticity, such as PIB-PB-0.3 and PS-DOP, which exhibit $\log_{10}(Ec_e) \gtrsim -1.5$ during capillary breakup, a size-independent exponential decay in the EC stage may occur. This implies that a nearly constant apparent relaxation time can be observed. In contrast, fluids with relatively high surface tension and low viscoelasticity, such as water-based dilute solutions like PEO-PEG and PEOvis, exhibit significant size dependence of the apparent relaxation time. The extensibility b determines the value of

the critical Ec_e at which this effect occurs, with smaller b making this influence more readily triggered. Additionally, we speculate that in micro-scale capillary breakup processes (e.g., within biological tissues), where Ec_e is extremely small, the linear dependence of $\lambda_e \sim D_0$ is likely to occur.

In summary, our study reveals, through experiments and numerical solutions, how inevitable pre-stretching during the visco-capillary stage of capillary breakup influences the exponential decay in the elasto-capillary stage and the apparent relaxation time λ_e obtained using classical formulations for viscoelastic fluids. Through a theoretical model, we demonstrate that the apparent relaxation time is always smaller than the actual relaxation time, i.e., $\lambda_e < \lambda$. We further identify that the size dependence of λ_e is governed by the extensibility b , solvent viscosity ratio β , and the dimensionless number $Ec_e = D_0\eta_p/(2\gamma\lambda_e)$. Large b and Ec_e result in size-independent behavior, while under small Ec_e conditions, the scaling $\lambda_e \sim D_0 \sim \ell$ emerges. We present a methodology for determining the actual relaxation time λ by synthesizing a series of apparent relaxation times λ_e measured under various size conditions. These findings provide a new perspective on accurately measuring viscoelastic properties using capillary breakup rheometry and offer insights into the size effects in the capillary breakup dynamics of viscoelastic fluids. Looking forward, several factors need to be considered to address the measurement of more complex fluids, such as those with shear-thinning viscosity, fluids where the IC stage dominates instead of the VC stage.

We thank Evgeniy Boyko for valuable discussions. We thank the NSF-supported project (NSF-BSF: Explaining the Mismatch of Experiments and Simulations for Viscoelastic Flows, 2246791) and the Princeton Materials Research Science and Engineering Center (MRSEC, DMR-2011750) for partially funding this work. J.H. acknowledges the Kwanjeong Educational Foundation Graduate Fellowship for financial support.

* nh0529@princeton.edu

† hastone@princeton.edu

- [1] J. Eggers, *Rev. Mod. Phys.* **69**, 865–930 (1997).
- [2] G. H. McKinley, in *Rheology Reviews* (British Society of Rheology, Aberystwyth, 2005), pp. 1–49.
- [3] B. Keshavarz, E. C. Houze, J. R. Moore, M. R. Koerner, and G. H. McKinley, *Phys. Rev. Lett.* **117** (2016), 10.1103/physrevlett.117.154502.
- [4] V. Entov and E. Hinch, *J. Non-Newtonian Fluid Mech.* **72**, 31–53 (1997).
- [5] Y. Amarouchene, D. Bonn, J. Meunier, and H. Kellay, *Phys. Rev. Lett.* **86**, 3558–3561 (2001).
- [6] J. Eggers, M. A. Herrada, and J. H. Snoeijer, *J. Fluid Mech.* **887** (2020), 10.1017/jfm.2020.18.
- [7] A. Deblais, M. A. Herrada, J. Eggers, and D. Bonn, *J. Fluid Mech.* **904** (2020), 10.1017/jfm.2020.765.
- [8] C. Wagner, Y. Amarouchene, D. Bonn, and J. Eggers, *Phys. Rev. Lett.* **95** (2005), 10.1103/physrevlett.95.164504.
- [9] P. P. Bhat, S. Appathurai, M. T. Harris, M. Pasquali, G. H. McKinley, and O. A. Basaran, *Nat. Phys.* **6**, 625 (2010).
- [10] A. Deblais, K. Velikov, and D. Bonn, *Phys. Rev. Lett.* **120** (2018), 10.1103/physrevlett.120.194501.
- [11] E. Turkoz, J. M. Lopez-Herrera, J. Eggers, C. B. Arnold, and L. Deike, *J. Fluid Mech.* **851** (2018), 10.1017/jfm.2018.514.
- [12] L. E. Rodd, T. P. Scott, J. J. Cooper-White, and G. H. McKinley, *Appl. Rheol.* **15**, 12 (2005).
- [13] F. Ingremeau and H. Kellay, *Phys. Rev. X* **3** (2013), 10.1103/physrevx.3.041002.
- [14] V. Calabrese, A. Q. Shen, and S. J. Haward, *Macromolecules* **57**, 9668–9676 (2024).
- [15] S. L. Anna and G. H. McKinley, *J. Rheol.* **45**, 115–138 (2001).
- [16] G. H. McKinley and T. Sridhar, *Annu. Rev. Fluid Mech.* **34**, 375–415 (2002).
- [17] A. Aisling, R. Saraka, and N. J. Alvarez, *J. Non-Newtonian Fluid Mech.* **333**, 105321 (2024).
- [18] A. Gaillard, M. A. Herrada, A. Deblais, J. Eggers, and D. Bonn, *Phy. Rev. Fluids* **9** (2024), 10.1103/physrevfluids.9.073302.
- [19] J. Eggers and E. Villermaux, *Rep. Prog. Phys.* **71**, 036601 (2008).
- [20] A. M. Ardekani, V. Sharma, and G. H. McKinley, *J. Fluid Mech.* **665**, 46–56 (2010).
- [21] V. Sharma, S. J. Haward, J. Serdy, B. Keshavarz, A. Soderlund, P. Threlfall-Holmes, and G. H. McKinley, *Soft Matter* **11**, 3251 (2015).
- [22] B. Keshavarz, V. Sharma, E. C. Houze, M. R. Koerner, J. R. Moore, P. M. Cotts, P. Threlfall-Holmes, and G. H. McKinley, *J. Non-Newtonian Fluid Mech.* **222**, 171–189 (2015).
- [23] S. Rajesh, V. Thiévenaz, and A. Sauret, *Soft Matter* **18**, 3147–3156 (2022).
- [24] P. Bazazi, H. A. Stone, and S. H. Hejazi, *Phys. Rev. Lett.* **130** (2023), 10.1103/physrevlett.130.034001.
- [25] J. Dinic, L. N. Jimenez, and V. Sharma, *Lab Chip* **17**, 460 (2017).
- [26] J. Dinic, M. Biagioli, and V. Sharma, *J. Polym. Sci. Part B: Polym. Phys.* **55**, 1692–1704 (2017).
- [27] L. N. Jimenez, J. Dinic, N. Parsi, and V. Sharma, *Macromolecules* **51**, 5191 (2018).
- [28] K. Zinelis, T. Abadie, G. H. McKinley, and O. K. Matar, *Soft Matter* **20**, 8198–8214 (2024).
- [29] J. Dinic and V. Sharma, *Proc. Natl. Acad. Sci. USA* **116**, 8766 (2019).
- [30] O. Arnolds, H. Buggisch, D. Sachsenheimer, and N. Willenbacher, *Rheol. Acta* **49**, 1207 (2010).
- [31] J. Dinic, Y. Zhang, L. N. Jimenez, and V. Sharma, *ACS Macro Lett.* **4**, 804 (2015).
- [32] K. Zinelis, T. Abadie, G. H. McKinley, and O. K. Matar, *Soft Matter* **20**, 8198–8214 (2024).
- [33] “Supplemental material,” See Supplemental Material at [URL] for additional rheological and experimental characterizations, as well as theoretical calculations.